

Accelerated quantum control in a three-level system by jumping along the geodesics

Musang Gong^{1,2}, Min Yu^{1,2}, Ralf Betzholtz^{1,2}, Yaoming Chu^{1,2},
Pengcheng Yang^{1,2,*}, Zhenyu Wang^{3,4} and Jianming Cai^{1,2,5}

¹*School of Physics, Hubei Key Laboratory of Gravitation and Quantum Physics,
Institute for Quantum Science and Engineering, Huazhong University of Science and Technology, Wuhan 430074, China*

²*International Joint Laboratory on Quantum Sensing and Quantum Metrology,
Huazhong University of Science and Technology, Wuhan 430074, China*

³*Guangdong Provincial Key Laboratory of Quantum Engineering and Quantum Materials,
School of Physics and Telecommunication Engineering,
South China Normal University, Guangzhou 510006, China*

⁴*Frontier Research Institute for Physics, South China Normal University, Guangzhou 510006, China*

⁵*Shanghai Key Laboratory of Magnetic Resonance, East China Normal University, Shanghai 200062, China*

In a solid-state spin system, we experimentally demonstrate a protocol for quantum-state population transfer with an improved efficiency compared to traditional stimulated Raman adiabatic passage (STIRAP). Using the ground state triplet of the nitrogen-vacancy center in diamond, we show that the required evolution time for high-fidelity state transfer can be reduced by almost one order of magnitude. Furthermore, we establish an improved robustness against frequency detuning caused by magnetic noise as compared to STIRAP. These results provide a powerful tool for coherent spin manipulation in the context of quantum sensing and quantum computation.

I. INTRODUCTION

Coherent control and manipulation with a high fidelity of the quantum state of a system has long been the subject of intensive research in modern quantum technologies, such as coherent manipulation of atomic and molecular systems [1, 2], quantum information processing [3–5], and high-precision measurement [6–9]. There is a vast literature proposing and implementing various methods for this purpose, such as adiabatic-passage techniques [10–13], which are robust against variations of the control fields [14–18] and have been widely applied, in quantum-state engineering [19], quantum simulation [20–22], and quantum computation [23, 24], to mention only a few.

Among these adiabatic-passage techniques, stimulated Raman adiabatic passage (STIRAP) [25, 26] is a paradigm example for adiabatic population transfer between two distinct states in a three-state system without populating the intermediate state using two control fields. Due to the robustness against control-parameter perturbations and the relaxation through spontaneous emission of the intermediate state, STIRAP has been extensively used in the realization of various quantum-information-processing tasks [27–30]. However, such adiabatic methods are based on the adiabatic theorem of quantum mechanics [31] and can thereby be time-consuming due to the necessity to fulfill the adiabatic condition

$$\left| \frac{\langle \phi_m(t) | \dot{H}(t) | \phi_n(t) \rangle}{[E_n(t) - E_m(t)]^2} \right| \ll 1, \quad (1)$$

where $|\phi_m(t)\rangle$ and $|\phi_n(t)\rangle$ denote the eigenstates of the time-dependent Hamiltonian $H(t)$ with the corresponding eigenenergies $E_m(t)$ and $E_n(t)$, whereas $\dot{H}(t)$ represents the time

derivative of $H(t)$. This condition requires a slow driving in order to ensure that the system remains in an instantaneous eigenstate throughout the process. Therefore, considerable attention has been focused on methods to speed up adiabatic processes, both theoretically [32–39] and experimentally in various platforms [40–48].

Remarkably, the possibility of a quantum adiabatic evolution even in the presence of vanishing energy gaps has been demonstrated theoretically [49] and experimentally [44], respectively. The proposed method is a protocol employing discrete jumps along the evolution path of the control parameters to realize quantum adiabatic processes at unlimited rates in a two-level system. Such a jump protocol enables a rapid evolution that can even avoid path points where the eigenstates of the Hamiltonian are not experimentally feasible [49].

Among the platforms for practical implementations of quantum technologies at ambient conditions, the negatively charged nitrogen-vacancy (NV) center in diamond [50, 51] represents an appealing and promising candidate, due to its long coherence time at room temperature and well developed coherent control techniques [52–58]. Therefore, the NV system has a great number of applications in quantum information processing [59–66] and quantum computing [67, 68]. Besides other favorable properties, the energy-level structure of the NV center [69, 70] makes it a quantum-sensing platform for temperature [71–74], strain [75–77], electric [78] and magnetic fields [79–81], as well as a hybrid sensor [82–84].

In this work, we utilize a single NV center to experimentally implement a jump protocol in a three-level system [85] to speed up the adiabatic state transfer by jumping along the geodesics in the three-level system. To demonstrate the speed up, we compare the population transfer to the well-established STIRAP. We find that the jump scheme exhibits a high transfer efficiency at appreciably shorter times. Furthermore, we demonstrate that it is robust against environmental magnetic noise, which illustrates the feasibility of the jump protocol in realistic environments.

* pcyang@hust.edu.cn

II. JUMP PROTOCOL

The conventional quantum adiabatic theorem requires the evolution of the quantum systems to be subject to slowly varying Hamiltonians, which imposes a speed limit on quantum adiabatic methods. On the other hand, due to the limited coherence time of quantum systems, a fast coherent control is desired in order to attain high operation fidelities. Therefore, intensive work has been done to develop new methods to improve the efficiency of quantum adiabatic processes. In Ref. [49], a method was proposed in which the adiabatic evolution is decomposed into a product of gauge-invariant unitary operators and a necessary and sufficient condition for adiabaticity is provided. This, in turn, has prompted a new scheme utilizing parametrized pulse sequences to improve the speed of the adiabatic evolution [44].

In this Letter, we consider a system comprised of the three states $| - 1 \rangle$, $| 0 \rangle$, and $| + 1 \rangle$ where there is no direct transition between the two states $| - 1 \rangle$ and $| + 1 \rangle$ [see Fig. 1(a)] and which is described by the parametrized Hamiltonian $H(\theta)$. Here, let the parameter $\theta = \theta(t)$ be a dimensionless time-dependent monotonic function with the initial condition $\theta(t = 0) = 0$. Our aim is to realize an adiabatic population transfer between $| - 1 \rangle$ and $| + 1 \rangle$ by variation of the parameter θ . We denote the instantaneous eigenstates and eigenenergies of $H(\theta)$ by $\{|n(\theta)\rangle\}$ and $\{E_n(\theta)\}$, respectively.

According to Ref. [85], for a total evolution time T the time-evolution operator $U(T)$ generated by $H(\theta)$, from $t = 0$ to $t = T$, can be written as the product

$$U(T) = U_{\text{adia}} U_{\text{Dia}}(T), \quad (2)$$

where U_{adia} is the time-evolution operator of the ideal adiabatic process, whereas the undesirable nonadiabatic correction reads

$$U_{\text{Dia}}(T) = \mathcal{P} \exp \left[i \int_0^{\theta_T} X(\theta) d\theta \right], \quad (3)$$

with the shorthand $\theta_T \equiv \theta(t = T)$. Furthermore, \mathcal{P} represents the path-ordering operation [85, 86] with respect to the parameter θ , in the same fashion as the well-known time-ordering operator [87]. Lastly, we have also defined the quantity

$$X(\theta) = \sum_{n,m} \xi_{n,m}(\theta) G_{n,m}(\theta) \quad (4)$$

in terms of

$$\xi_{n,m}(\theta) = \exp\{i[\varphi_n(\theta) - \varphi_m(\theta)]\}, \quad (5)$$

$$G_{n,m}(\theta) = \langle n(\theta) | i \frac{d}{d\theta} | m(\theta) \rangle | n(0) \rangle \langle m(0) | \quad (6)$$

with the dynamical phases $\varphi_j(\theta) = \int_0^\theta E_j(t') dt'$. Thus, from Eq. (2) we see that if $U_{\text{Dia}}(T)$ equals the identity operator I , all nonadiabatic effects are eliminated.

We would like to realize an adiabatic transfer by a dark state, $|d(\theta)\rangle$, which is absent in the Hamiltonian $H(\theta)$ and

corresponds to an eigenstate with a zero eigenvalue. If we choose $| - 1 \rangle$ as the initial dark state, the initial Hamiltonian takes the form $H(\theta = 0) = \Omega|0\rangle\langle -1| + \text{H.c.} + \Delta|0\rangle\langle 0|$, where Ω is the amplitude and Δ is the detuning. The value of Δ can be used to optimize the performance when there are dissipation and/or decoherence on both the intermediate state $|0\rangle$ and the qubit sub-space $\{| \pm 1 \rangle\}$ [85]. For simplicity, here we consider $\Delta = 0$, as it allows for a faster control, such that possible detrimental effects of decoherence on $\{| \pm 1 \rangle\}$ can be minimized. The eigenstates of $H(\theta = 0)$ are $|d(0)\rangle = | - 1 \rangle$ and $|\mu_\pm(0)\rangle = (| + 1 \rangle \pm |0\rangle)/2$.

As in STIRAP, choosing the dark state to have the form

$$|d(\theta)\rangle = \sin(\theta)| + 1 \rangle + \cos(\theta)| - 1 \rangle, \quad (7)$$

we find that $|d(\theta)\rangle = \exp(-iG\theta)|d(0)\rangle$, with the constant generator $G = i| - 1 \rangle\langle + 1| - i| + 1 \rangle\langle - 1|$. We note that $dG/d\theta = 0$, which results in the important property that the $G_{n,m}$ in Eq. (6) are all constant [85] if we use the eigenstates $\{|n(\theta)\rangle\} = \{|d(\theta)\rangle, |\mu_\pm(\theta)\rangle\}$ of the Hamiltonian

$$\begin{aligned} H(\theta) &= \exp(-iG\theta)H(0)\exp(iG\theta), \\ &= \Omega|\mu_+(\theta)\rangle\langle\mu_+(\theta)| - \Omega|\mu_-(\theta)\rangle\langle\mu_-(\theta)|, \\ &= \Omega[\cos(\theta)| + 1 \rangle - \sin(\theta)| - 1 \rangle]\langle 0| + \text{H.c.}, \end{aligned} \quad (8)$$

where $|\mu_\pm(\theta)\rangle = \exp(-iG\theta)|\mu_\pm(0)\rangle$. We can derive the relation [85]

$$G_{n,m} = \langle n(0) | G | m(0) \rangle | n(0) \rangle \langle m(0) |, \quad (9)$$

which also shows that Eq. (6) becomes a constant.

Now, we apply $H(\theta)$ for a duration $\tau = \pi/\Omega$ at N equally-spaced points $\theta = \theta_1, \theta_2, \dots, \theta_N$ between $\theta_0 = 0$ and $\theta_T = \theta_{N+1} \equiv \pi/2$. Specifically, we choose the N parameter values θ_j ($j = 1, \dots, N$) to be

$$\theta_j = \frac{2j-1}{N} \frac{\pi}{4}. \quad (10)$$

The time-evolution operator thereby becomes $U(T) = \exp[-iH(\theta_N)\tau] \exp[-iH(\theta_{N-1})\tau] \dots \exp[-iH(\theta_1)\tau]$. Additionally, we find $\xi_{d,\mu_+}(\theta) = \xi_{d,\mu_-}(\theta) = F(\theta)$, with

$$F(\theta) = (-1)^j, \quad (11)$$

$\theta \in [\theta_j, \theta_{j+1})$, since applying $H(\theta)$ in Eq. (8) with a fixed value of θ for a time $\tau = \pi/\Omega$ yields a shift of $\pm\pi$ between the dynamic phases of $|\mu_\pm(\theta)\rangle$ and $|d(\theta)\rangle$. On the other hand, evaluating Eq. (9) shows $G_{n,n} = G_{\mu_+,\mu_-} = G_{\mu_-,\mu_+} = 0$. Equation (3) thus takes the form

$$U_{\text{Dia}}(T) = \exp \left[i \left(\sum_{n=\mu_\pm} G_{n,d} + \text{H.c.} \right) \int_0^{\theta_T} F(\theta) d\theta \right], \quad (12)$$

which finally reveals $U_{\text{Dia}}(T) = I$ by using Eqs. (10) and (11). This means our choice of parameter jumps realizes the desired adiabatic evolution $U(T) = U_{\text{adia}}$ in the finite time $T = N\tau$.

III. PERFORMANCE OF THE JUMP PROTOCOL

To demonstrate the high population transfer efficiency that can be achieved with this jump protocol, we experimentally compare it with a traditional STIRAP protocol in an NV-center system. The STIRAP protocol utilizes two Raman pulses to realize the population transfer between two states under the adiabatic condition. In our case, we use Raman pulses with a Gaussian envelope. Both optical and microwave fields can be used for coherent control in the NV center system, we implement the STIRAP protocol by microwave fields whose amplitude and phase are allowed to be better controlled.

In the experiment, we choose the ground-state triplet of a single NV center as the three-level system, respectively identifying $|0\rangle$ and $|\pm 1\rangle$ with the $m_s = 0$ and $m_s = \pm 1$ states. The degeneracy of the $m_s = \pm 1$ states is lifted by an external magnetic field aligned with the NV-center axis. An acousto-optical modulator (AOM) is used to control the 532-nm green laser which is employed for the optical ground-state initialization and the readout of the spin state. In order to manipulate the spin states, we apply two microwave driving fields which are resonant with the $|0\rangle \leftrightarrow |\pm 1\rangle$ transitions through an arbitrary waveform generator (AWG). The Rabi frequencies of the two driving fields are denoted by Ω_{\pm} .

In the interaction picture with respect to the NV-center ground-state Hamiltonian, the three-level system is described by the Hamiltonian in Eq. (8). The parameter Ω and the Rabi frequencies Ω_{\pm} of the microwave driving fields are related by $\Omega_- = 2\Omega \sin(\theta)$ and $\Omega_+ = 2\Omega \cos(\theta)$. By changing Ω_- and Ω_+ via the AWG, while keeping $\Omega_-^2 + \Omega_+^2$ constant, we are able to tune the value of θ . In the experiment, we set $\Omega/2\pi = 4$ MHz and since the duration τ of each control step with θ_j in the jump protocol should be equal to π/Ω in order to fulfill the adiabatic condition we use $\tau = 0.125 \mu\text{s}$.

Figure 1 shows a schematic of the experimental setup. Figure 1(a) depicts the energy-level structure of the NV ground state. Here, the energy splitting δ , with the gyromagnetic ratio $\gamma/2\pi = 2.8$ MHz/G, between the states $|m_s = \pm 1\rangle$ stems from the Zeeman effect due to the applied magnetic field B . The explicit setup is sketched in Fig. 1(b) and Fig. 1(c) shows the pulse sequences we apply. The upper part depicts the sequence for the STIRAP protocol we will use for comparison, whereas the lower one represents the sequence for the jump protocol. Since we aim to measure the transfer efficiency in the three-level system, the pulses sequences consists of two parts, namely parts I and II, from which we can infer the transfer efficiency given by the population of $|+1\rangle$. In detail, both sequences begin with laser 1 to initialize the state in $|0\rangle$ followed by a π pulse on the $|0\rangle \leftrightarrow |-1\rangle$ transition. Then the actual protocols of length T are applied, where the building blocks J_j represent the N control steps of θ in the jump protocol. Laser 2 reads out the population of $|0\rangle$ at the end of part I and, at the same time, re-initializes the electron spin for part II, which differs only by an additional π pulse before read-out, such that the population of $|-1\rangle$ is measured.

To demonstrate the applicability of the jump protocol we measure the population transfer from $|-1\rangle$ to $|+1\rangle$ by tracking the population of all three state of the system in

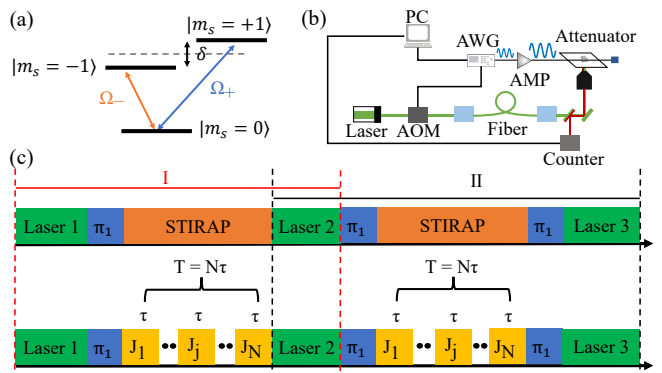


FIG. 1. (a) The energy difference $\delta = \gamma B$ between $m_s = \pm 1$ arises from the Zeeman effect. (b) The experiment setup for the coherent control of the NV center. (c) Upper part: pulse sequence for the STIRAP protocol used as comparison. Lower part: pulse sequence for the jump protocol. Parts I and II measure the population of $|0\rangle$ and $|-1\rangle$, respectively. Laser initialization and readout are the same for both schemes. π_1 corresponds to π pulses on the transition $|0\rangle \leftrightarrow |-1\rangle$. In the jump protocol, there are N successive control pulses of length τ , represented by J_j , that correspond to the piecewise constant values θ_j .

dependence of the total evolution time T for different numbers of pulses. For a given value of T each of the N pulses thereby has the length T/N . This is shown in Fig. 2, where Figs. 2(a)–2(d) respectively depict the four pulse numbers $N = 1, 2, 3, 4$, corresponding to the final values of the evolution times $T = 125, 250, 375, 500$ ns. Here, the markers are experiment results, whereas solid lines show numerical simulation. We find a good agreement and the results show that the duration of 125 ns for a single-pulse protocol leads to a full population transfer. It can also be seen that the population in the target state $|+1\rangle$ with a value close to unity has a wider range at the end of the protocol for larger N , which indicates the robustness of multiple-pulse protocols with respect to amplitude imperfections.

We now compare the performance of the jump protocol to the well-established STIRAP protocol. Details on the STIRAP measurements are given in the Appendix. For better comparison, in Fig. 3(a), we show the transfer efficiency, as given by the population of $|+1\rangle$, for $N = 1, 2, 3, 4$ [corresponding to the black data from Figs. 2(a)–2(d)]. Figure 3(b), on the other hand, shows the results of the STIRAP protocol for three different evolution times, namely $T = 500, 1200, 1800$ ns. For the shortest evolution time, which is the longest we use for the jump protocol, the transfer efficiency only reaches around 60%. With the parameters we chose, i.e., a maximum amplitude of the Raman control pulses of 2Ω , the time required for a complete population transfer is well above 1000 ns and thereby appreciably longer than the one required in the jump protocol. In both Figs. 3(a) and 3(b), markers and solid lines represent experimental and numerical simulation results, respectively.

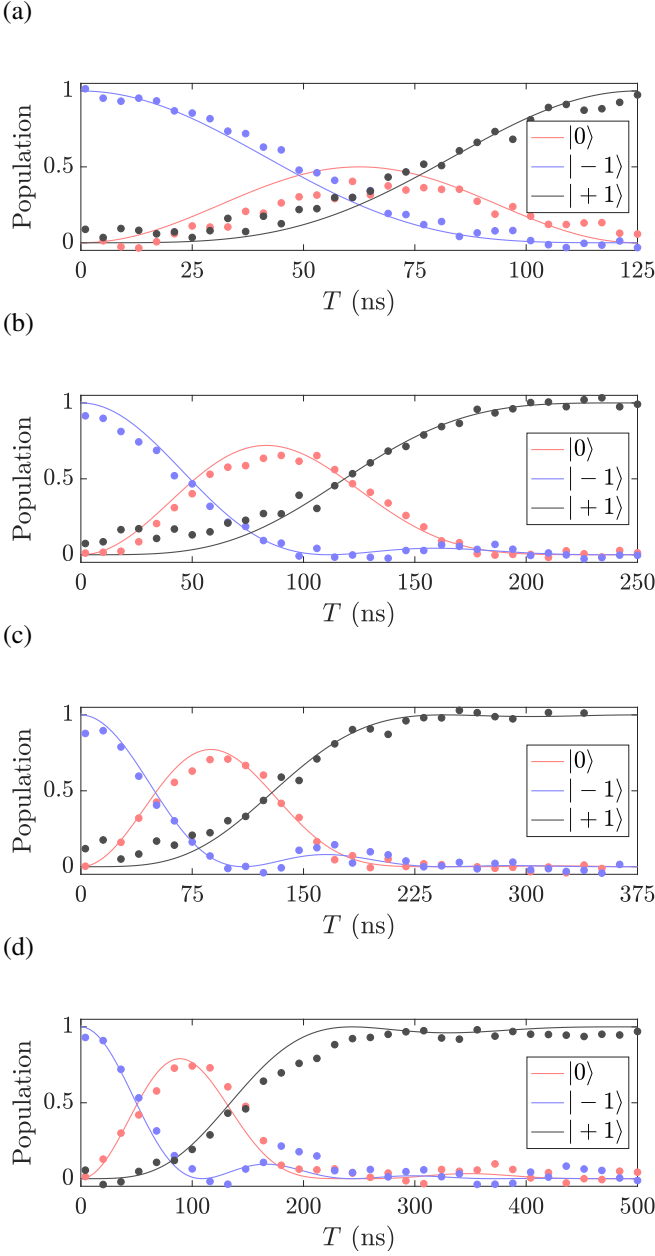


FIG. 2. Dependence of the populations of the three-level system on the total evolution time T in the jump protocol. (a)-(d) respectively correspond to $N = 1, 2, 3, 4$ control pulses with $\Omega/2\pi = 4$ MHz. For every value of T each of the N pulses has the length T/N . Markers show experimental results and solid lines are numerical simulations.

IV. ROBUSTNESS AGAINST NOISE

Finally, we demonstrate the robustness of the jump protocol against environmental noise. In the solid-state spin system, the main source of noise is the surrounding bath of nuclear spins which can be described by an effective magnetic field [89]. To investigate the detrimental effects of static magnetic field noise, we artificially add a detuning $\pm\Delta$ between the microwave driving fields and the transitions $|0\rangle \leftrightarrow |\mp 1\rangle$,

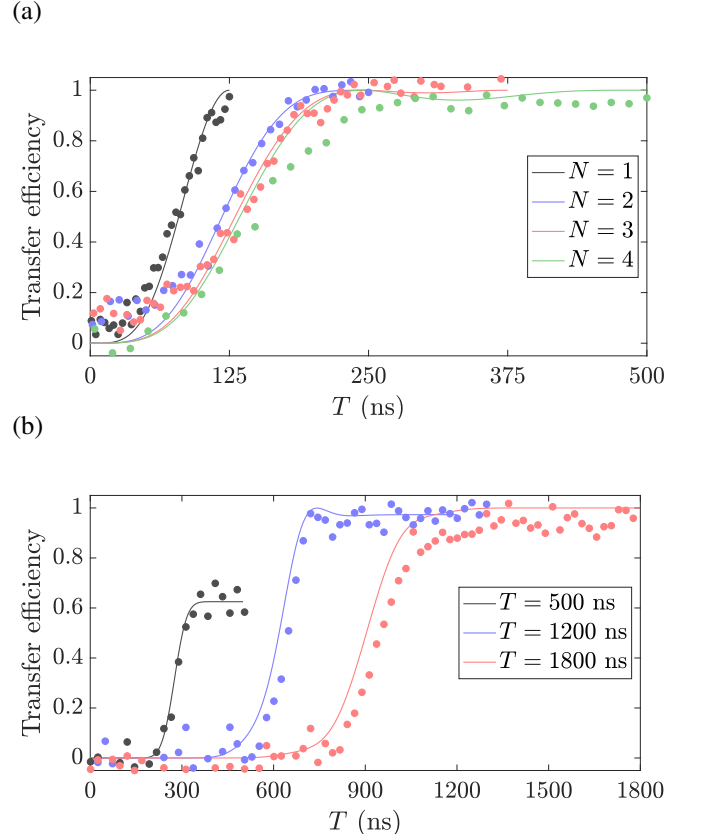


FIG. 3. Comparison of the transfer efficiency between the jump protocol and STIRAP. (a) Different number of control pulses, $N = 1, 2, 3, 4$, of the jump protocol. (b) STIRAP for different final evolution times, $T = 500, 1200, 1800$ ns. Markers and solid lines represent experimental data and numerical simulations, respectively.

while keeping the remaining parameters unchanged. We then compare the robustness of the transfer efficiency of the jump protocol to the one of the STIRAP. In this case, the Hamiltonian for the jump and STIRAP protocol respectively read

$$H_I = \begin{pmatrix} 0 & \Omega \cos \phi & \Omega \sin \phi \\ \Omega \cos \phi & \Delta & 0 \\ \Omega \sin \phi & 0 & -\Delta \end{pmatrix}, \quad (13)$$

$$H_{\text{STIRAP}} = \frac{1}{2} \begin{pmatrix} 0 & \Omega_P(t) & \Omega_S(t) \\ \Omega_P(t) & \Delta & 0 \\ \Omega_S(t) & 0 & -\Delta \end{pmatrix}. \quad (14)$$

For the comparison of the two schemes, we again set the frequency $\Omega/2\pi = 4$ MHz and chose $N = 4$ as the number of control pulses. This implies a total evolution time of $T = 500$ ns, which we also set as the total duration of the STIRAP protocol. The maximal amplitudes of the pump and Stokes pulses, $\Omega_P(t)$ and $\Omega_S(t)$, in the STIRAP are both given by 2Ω . The experiment results for varying the detuning $\Delta/2\pi$ from -2 MHz through 2 MHz are shown in Fig. 4. Solid lines represent simulation results whereas the markers with error bars show experimental results. As one sees, for

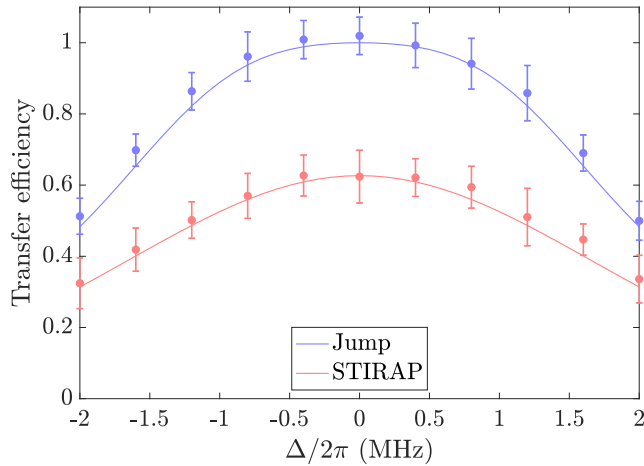


FIG. 4. Comparison of the robustness against frequency detuning between the jump protocol (blue) and STIRAP (red). The evolution time is $T = 500$ ns for both cases ($N = 4$ in the jump protocol). Markers with error bars and solid lines represent experimental data and numerical simulations, respectively.

the same evolution time, the jump scheme exhibits not only a higher transfer efficiency throughout the whole range of the detuning, but also a much flatter central part, indicating a better robustness than the STIRAP.

V. CONCLUSIONS

We have demonstrated jump scheme for population transfer in a three-level system realized in single NV-center spin in diamond. By comparing the protocol to a traditional STIRAP scheme, we have shown its significant advantages. In particular, the state-transfer speed and efficiency is greatly improved, i.e., much shorter times are required to achieve a high-fidelity population transfer. Furthermore, we have also compared the impact of noise on the two schemes under the same evolution time and established an improved robustness of the jump protocol. The developed method is thereby a promising candidate for practical applications in quantum control, quantum sensing, quantum information processing, and even chemical interaction control.

ACKNOWLEDGMENTS

We thank Dongxiao Li for discussions and help during the initial stage of manuscript preparation. R. B. is grateful to S. Schein for helpful comments. This work is supported by the National Natural Science Foundation of China (Grants No. 12161141011, No. 11874024, and No. 12074131), the National Key R&D Program of China (Grant No. 2018YFA0306600), the Shanghai Key Laboratory of Magnetic Resonance (East China Normal University), and the Natural Science Foundation of Guangdong Province (Grant No. 2021A1515012030).

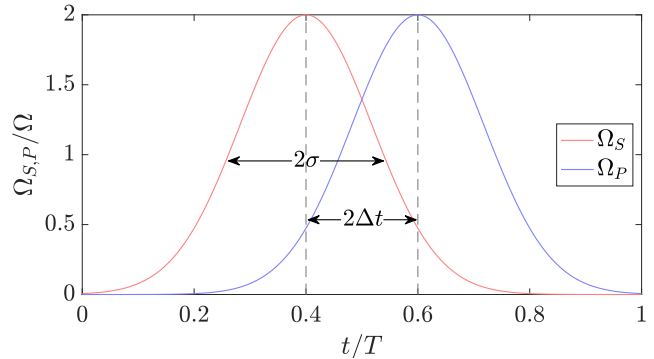


FIG. 5. The two Raman pulses in the STIRAP scheme. The red and blue lines correspond to the control pulses $\Omega_S(t)$ and $\Omega_P(t)$, respectively. Both pulses have a Gaussian envelope with the full-width at half-maximum 2σ and the peak value 2Ω . They partially overlap and the delay between them is $2\Delta t$.

Appendix A: STIRAP

To achieve the population transfer through an auxiliary state in the STIRAP, one utilizes two Raman control pulses with the envelopes $\Omega_S(t)$ and $\Omega_P(t)$, called the Stokes and pump pulses. The NV-center ground state consists of three sub-levels, $m_s = 0, \pm 1$. The states $|0\rangle$ and $|\pm 1\rangle$ are coupled, whereas $|-1\rangle \leftrightarrow | + 1\rangle$ is a forbidden transition. Thus, the primary aim of STIRAP is to drive the $|-1\rangle \leftrightarrow | + 1\rangle$ transition using $|0\rangle$ as an auxiliary state without or with only minimal population loss to the latter state. The two Raman pulses are implemented with microwave fields in our experiment.

The NV-center spin is prepared in the state $|-1\rangle$ by applying a π -pulse on the $|0\rangle \leftrightarrow |-1\rangle$ transition after optical initialization. We then apply two resonant microwave control pulses with the envelopes $\Omega_S(t)$ and $\Omega_P(t)$ for the population transfer to $| + 1\rangle$. The Stokes pulse $\Omega_S(t)$ is applied first to drive the transition $|0\rangle \leftrightarrow | + 1\rangle$ and is followed by the pump pulse $\Omega_P(t)$ which drives the transition $|0\rangle \leftrightarrow |-1\rangle$. In the interaction picture with respect to the ground-state Hamiltonian, the Hamiltonian of STIRAP scheme is given by

$$H_{\text{STIRAP}} = \frac{1}{2} \begin{pmatrix} 0 & \Omega_P(t) & \Omega_S(t) \\ \Omega_P(t) & 0 & 0 \\ \Omega_S(t) & 0 & 0 \end{pmatrix} \quad (\text{A1})$$

in the basis $\{|0\rangle, |-1\rangle, | + 1\rangle\}$.

The two Raman control pulses are applied adiabatically and partially overlap to completely transfer the population, see Fig. 5. They have Gaussian shapes and for a total evolution time T they are centered at $T/2 \pm \Delta t$, i.e., the second pulse is delayed by $2\Delta t$. Furthermore, their full-width at half-maximum is 2σ and their maximal value is 2Ω . This means they have the form $\Omega_S(t) = 2\Omega \exp[-(t - T/2 + \Delta t)^2/\sigma^2]$ and $\Omega_P(t) = 2\Omega \exp[-(t - T/2 - \Delta t)^2/\sigma^2]$. In our experiment, we set $\Omega/2\pi = 4$ MHz, $\Delta t = T/10$, and $\sigma = T/6$.

After the adiabatic evolution, a green laser is applied to per-

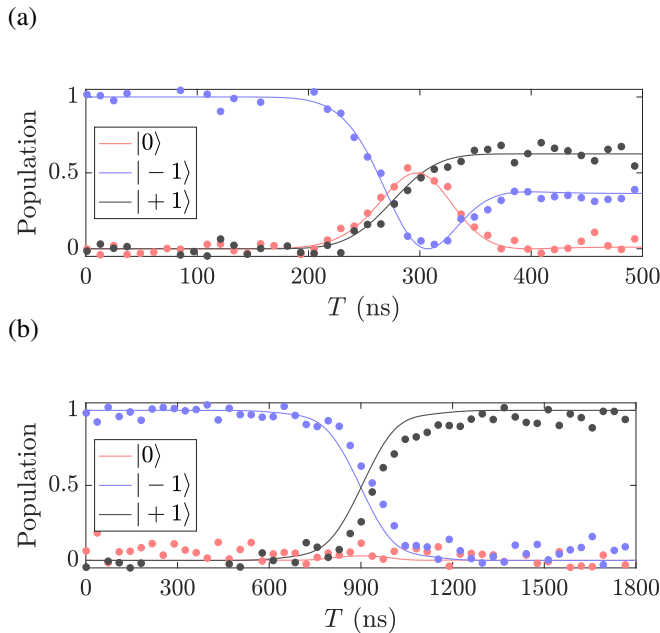


FIG. 6. Evolution of the populations of the three-level system in the STIRAP protocol. (a) and (b) respectively correspond to $T = 500$ ns and $T = 1800$ ns. The maximum of the two control-pulse envelopes $\Omega_S/2\pi$ and $\Omega_P/2\pi$ is both 8 MHz. Markers show experimental results and solid lines are numerical simulations.

form a fluorescence measurement and re-initialization. Then we repeat the pulse sequence adding a second π -pulse before the laser pulse [see Fig. 1(c) of the main text]. Combining the two fluorescence measurement results, one can obtain the population of all three states and thereby the state transfer efficiency. The full dynamics of the populations throughout the STIRAP process are shown in Fig. 6 for the two evolution times $T = 500$ ns and $T = 1800$ ns. We find that $> 95\%$ transfer efficiency can be achieved when the evolution time is longer than 900 ns and the transfer efficiency only reaches around 60% for $T = 500$ ns.

-
- [1] P. Král, I. Thanopoulos, and M. Shapiro, Colloquium: Coherently controlled adiabatic passage, *Rev. Mod. Phys.* **79**, 53 (2007).
- [2] L. C. Bassett, F. J. Heremans, D. J. Christle, C. G. Yale, G. Burkard, B. B. Buckley, and D. D. Awschalom, Ultrafast optical control of orbital and spin dynamics in a solid-state defect, *Science* **345**, 1333 (2014).
- [3] E. Farhi, J. Goldstone, S. Gutmann, J. Lapan, A. Lundgren, and D. Preda, A quantum adiabatic evolution algorithm applied to random instances of an NP-complete problem, *Science* **292**, 472 (2001).
- [4] C. Monroe and J. Kim, Scaling the ion trap quantum processor, *Science* **339**, 1164 (2013).
- [5] S. Chen, M. Raha, C. M. Phenicie, S. Ourari, and J. D. Thompson, Parallel single-shot measurement and coherent control of solid-state spins below the diffraction limit, *Science* **370**, 592 (2020).
- [6] M. A. Kasevich, Coherence with atoms, *Science* **298**, 1363 (2002).
- [7] K. Kotru, D. L. Butts, J. M. Kinast, and R. E. Stoner, Large-Area Atom Interferometry with Frequency-Swept Raman Adiabatic Passage, *Phys. Rev. Lett.* **115**, 103001 (2015).
- [8] B. Buckley, G. Fuchs, L. Bassett, and D. Awschalom, Spin-light coherence for single-spin measurement and control in diamond, *Science* **330**, 1212 (2010).
- [9] C. Liu, W. Liu, S. Wang, H. Li, Z. Lv, F. Zhang, D. Zhang, J. Teng, T. Zheng, D. Li, M. Zhang, P. Xu, and Q. Gong, Super-resolution nanoscopy by coherent control on nanoparticle emission, *Sci. Adv.* **6**, eaaw6579 (2020).
- [10] M. Shapiro and P. Brumer, Coherent Control of Atomic, Molecular, and Electronic Processes, *Adv. At. Mol. Opt. Phys.* **42**, 287 (2000).
- [11] A. A. Rangelov, N. V. Vitanov, L. P. Yatsenko, B. W. Shore, T. Halfmann, and K. Bergmann, Stark-shift-chirped rapid-adiabatic-passage technique among three states, *Phys. Rev. A* **72**, 053403 (2005).
- [12] B. T. Torosov, S. Guérin, and N. V. Vitanov, High-Fidelity Adiabatic Passage by Composite Sequences of Chirped Pulses, *Phys. Rev. Lett.* **106**, 233001 (2011).
- [13] T. Kovachy, S.-w. Chiow, and M. A. Kasevich, Adiabatic-rapid-passage multiphoton Bragg atom optics, *Phys. Rev. A* **86**, 011606 (2012).
- [14] K. Bergmann, H. Theuer, and B. W. Shore, Coherent population transfer among quantum states of atoms and molecules, *Rev. Mod. Phys.* **70**, 1003 (1998).
- [15] A. Fubini, G. Falci, and A. Osterloh, Robustness of adiabatic passage through a quantum phase transition, *New J. Phys.* **9**, 134 (2007).
- [16] K. Kumar, A. Vepsäläinen, S. Danilin, and G. Paraoanu, Stimulated Raman adiabatic passage in a three-level superconducting circuit, *Nat. Commun.* **7**, 10628 (2016).
- [17] Y.-X. Du, Z.-T. Liang, Y.-C. Li, X.-X. Yue, Q.-X. Lv, W. Huang, X. Chen, H. Yan, and S.-L. Zhu, Experimental realization of stimulated Raman shortcut-to-adiabatic passage with cold atoms, *Nat. Commun.* **7**, 12479 (2016).
- [18] Y. P. Kandel, H. Qiao, S. Fallahi, G. C. Gardner, M. J. Manfra, and J. M. Nichol, Adiabatic quantum state transfer in a semiconductor quantum-dot spin chain, *Nat. Commun.* **12**, 1 (2021).
- [19] N. V. Vitanov, T. Halfmann, B. W. Shore, and K. Bergmann, Laser-induced population transfer by adiabatic passage techniques, *Annu. Rev. Phys. Chem.* **52**, 763 (2001).
- [20] A. Aspuru-Guzik, A. D. Dutoi, P. J. Love, and M. Head-

- Gordon, Simulated quantum computation of molecular energies, *Science* **309**, 1704 (2005).
- [21] K. Kim, M.-S. Chang, S. Korenblit, R. Islam, E. E. Edwards, J. K. Freericks, G.-D. Lin, L.-M. Duan, and C. Monroe, Quantum simulation of frustrated ising spins with trapped ions, *Nature (London)* **465**, 590 (2010).
- [22] J. D. Biamonte, V. Bergholm, J. D. Whitfield, J. Fitzsimons, and A. Aspuru-Guzik, Adiabatic quantum simulators, *AIP Adv.* **1**, 022126 (2011).
- [23] J. A. Jones, V. Vedral, A. Ekert, and G. Castagnoli, Geometric quantum computation using nuclear magnetic resonance, *Nature (London)* **403**, 869 (2000).
- [24] R. Barends, A. Shabani, L. Lamata, J. Kelly, A. Mezzacapo, U. L. Heras, R. Babbush, A. G. Fowler, B. Campbell, Y. Chen, Z. Chen, B. Chiaro, A. Dunsworth, E. Jeffrey, E. Lucero, A. Megrant, J. Y. Mutus, M. Neeley, C. Neill, P. J. J. O'Malley, C. Quintana, P. Roushan, D. Sank, A. Vainsencher, J. Wenner, T. C. White, H. Solano, E. Neven, and J. M. Martinis, Digitized adiabatic quantum computing with a superconducting circuit, *Nature (London)* **534**, 222 (2016).
- [25] U. Gaubatz, P. Rudecki, S. Schiemann, and K. Bergmann, Population transfer between molecular vibrational levels by stimulated Raman scattering with partially overlapping laser fields. A new concept and experimental results, *J. Chem. Phys.* **92**, 5363 (1990).
- [26] N. V. Vitanov, A. A. Rangelov, B. W. Shore, and K. Bergmann, Stimulated Raman adiabatic passage in physics, chemistry, and beyond, *Rev. Mod. Phys.* **89**, 015006 (2017).
- [27] Z. Kis and F. Renzoni, Qubit rotation by stimulated Raman adiabatic passage, *Phys. Rev. A* **65**, 032318 (2002).
- [28] H. Goto and K. Ichimura, Multiqubit controlled unitary gate by adiabatic passage with an optical cavity, *Phys. Rev. A* **70**, 012305 (2004).
- [29] S.-B. Zheng, Nongeometric Conditional Phase Shift via Adiabatic Evolution of Dark Eigenstates: A New Approach to Quantum Computation, *Phys. Rev. Lett.* **95**, 080502 (2005).
- [30] X. Lacour, N. Sangouard, S. Guérin, and H. R. Jauslin, Arbitrary state controlled-unitary gate by adiabatic passage, *Phys. Rev. A* **73**, 042321 (2006).
- [31] A. Messiah, *Quantum Mechanics* (Courier Corporation, North Chelmsford, 2014).
- [32] X. Chen, I. Lizuain, A. Ruschhaupt, D. Guéry-Odelin, and J. G. Muga, Shortcut to Adiabatic Passage in Two- and Three-Level Atoms, *Phys. Rev. Lett.* **105**, 123003 (2010).
- [33] L. Giannelli and E. Arimondo, Three-level superadiabatic quantum driving, *Phys. Rev. A* **89**, 033419 (2014).
- [34] Z.-T. Liang, X. Yue, Q. Lv, Y.-X. Du, W. Huang, H. Yan, and S.-L. Zhu, Proposal for implementing universal superadiabatic geometric quantum gates in nitrogen-vacancy centers, *Phys. Rev. A* **93**, 040305 (2016).
- [35] A. Baksic, H. Ribeiro, and A. A. Clerk, Speeding up Adiabatic Quantum State Transfer by Using Dressed States, *Phys. Rev. Lett.* **116**, 230503 (2016).
- [36] F. Petiziol, E. Arimondo, L. Giannelli, F. Mintert, and S. Wimberger, Optimized three-level quantum transfers based on frequency-modulated optical excitations, *Sci. Rep.* **10**, 2185 (2020).
- [37] D. Stefanatos and E. Paspalakis, Speeding up adiabatic passage with an optimal modified Roland–Cerf protocol, *J. Phys. A* **53**, 115304 (2020).
- [38] A. del Campo and K. Kim, Focus on shortcuts to adiabaticity, *New J. Phys.* **21**, 050201 (2019).
- [39] D. Guéry-Odelin, A. Ruschhaupt, A. Kiely, E. Torrontegui, S. Martínez-Garaot, and J. G. Muga, Shortcuts to adiabaticity: Concepts, methods, and applications, *Rev. Mod. Phys.* **91**, 045001 (2019).
- [40] J.-F. Schaff, P. Capuzzi, G. Labeyrie, and P. Vignolo, Shortcuts to adiabaticity for trapped ultracold gases, *New J. Phys.* **13**, 113017 (2011).
- [41] M. G. Bason, M. Viteau, N. Malossi, P. Huillery, E. Arimondo, D. Ciampini, R. Fazio, V. Giovannetti, R. Mannella, and O. Morsch, High-fidelity quantum driving, *Nat. Phys.* **8**, 147 (2012).
- [42] N. Malossi, M. G. Bason, M. Viteau, E. Arimondo, R. Mannella, O. Morsch, and D. Ciampini, Quantum driving protocols for a two-level system: From generalized Landau-Zener sweeps to transitionless control, *Phys. Rev. A* **87**, 012116 (2013).
- [43] J. Zhang, J. H. Shim, I. Niemeyer, T. Taniguchi, T. Teraji, H. Abe, S. Onoda, T. Yamamoto, T. Ohshima, J. Isoya, and D. Suter, Experimental Implementation of Assisted Quantum Adiabatic Passage in a Single Spin, *Phys. Rev. Lett.* **110**, 240501 (2013).
- [44] K. Xu, T. Xie, F. Shi, Z.-Y. Wang, X. Xu, P. Wang, Y. Wang, M. B. Plenio, and J. Du, Breaking the quantum adiabatic speed limit by jumping along geodesics, *Sci. Adv.* **5**, eaax3800 (2019).
- [45] M. Li, X. Tan, K. Dai, P. Zhao, H. Yu, and Y. Yu, Demonstration of superadiabatic population transfer in superconducting qubit, *Chin. Phys. B* **27**, 063202 (2018).
- [46] A. Vepsäläinen, S. Danilin, and G. S. Paraoanu, Superadiabatic population transfer in a three-level superconducting circuit, *Sci. Adv.* **5**, aau5999 (2019).
- [47] W. Zheng, Y. Zhang, Y. Dong, J. Xu, Z. Wang, X. Wang, Y. Li, D. Lan, J. Zhao, S. Li, X. Tan, and Y. Yu, Optimal control of stimulated Raman adiabatic passage in a superconducting qubit, *npj Quantum Inf.* **8**, 9 (2020).
- [48] W. Zheng, J. Xu, Z. Wang, Y. Dong, D. Lan, X. Tan, and Y. Yu, Accelerated quantum adiabatic transfer in superconducting qubits, *Phys. Rev. Applied* **18**, 044014.
- [49] Z.-Y. Wang and M. B. Plenio, Necessary and sufficient condition for quantum adiabatic evolution by unitary control fields, *Phys. Rev. A* **93**, 052107 (2016).
- [50] A. Gruber, A. Drabenstedt, C. Tietz, L. Fleury, J. Wrachtrup, and C. von Borczyskowski, Scanning confocal optical microscopy and magnetic resonance on single defect centers, *Science* **276**, 2012 (1997).
- [51] L. Rondin, J.-P. Tetienne, T. Hingant, J.-F. Roch, P. Maletinsky, and V. Jacques, Magnetometry with nitrogen-vacancy defects in diamond, *Rep. Prog. Phys.* **77**, 056503 (2014).
- [52] F. Jelezko, T. Gaebel, I. Popa, A. Gruber, and J. Wrachtrup, Observation of Coherent Oscillations in a Single Electron Spin, *Phys. Rev. Lett.* **92**, 076401 (2004).
- [53] N. Bar-Gill, L. M. Pham, A. Jarmola, D. Budker, and R. L. Walsworth, Solid-state electronic spin coherence time approaching one second, *Nat. Commun.* **4**, 1 (2013).
- [54] G. Balasubramanian, P. Neumann, D. Twitchen, M. Markham, R. Kolesov, N. Mizuochi, J. Isoya, J. Achard, J. Beck, J. Tisler, V. Jacques, P. R. Hemmer, F. Jelezko, and J. Wrachtrup, Ultralong spin coherence time in isotopically engineered diamond, *Nat. Mater.* **8**, 383 (2009).
- [55] Y. Chu, M. Markham, D. J. Twitchen, and M. D. Lukin, All-optical control of a single electron spin in diamond, *Phys. Rev. A* **91**, 021801 (2015).
- [56] Z. Shu, Y. Liu, Q. Cao, P. Yang, S. Zhang, M. B. Plenio, F. Jelezko, and J. Cai, Observation of Floquet Raman Transition in a Driven Solid-State Spin System, *Phys. Rev. Lett.* **121**, 210501 (2018).
- [57] J. Tian, H. Liu, Y. Liu, P. Yang, R. Betzholtz, R. S. Said,

- F. Jelezko, and J. Cai, Quantum optimal control using phase-modulated driving fields, *Phys. Rev. A* **102**, 043707 (2020).
- [58] Q.-Y. Cao, P.-C. Yang, M.-S. Gong, M. Yu, A. Retzker, M. Plenio, C. Müller, N. Tomek, B. Naydenov, L. McGuinness, F. Jelezko, and J.-M. Cai, Protecting Quantum Spin Coherence of Nanodiamonds in Living Cells, *Phys. Rev. Applied* **13**, 024021 (2020).
- [59] J. Wrachtrup and F. Jelezko, Processing quantum information in diamond, *J. Phys.: Condens. Matter* **18**, S807 (2006).
- [60] F. Dolde, I. Jakobi, B. Naydenov, N. Zhao, S. Pezzagna, C. Trautmann, J. Meijer, P. Neumann, F. Jelezko, and J. Wrachtrup, Room-temperature entanglement between single defect spins in diamond, *Nat. Phys.* **9**, 139 (2013).
- [61] J. Cai, A. Retzker, F. Jelezko, and M. B. Plenio, A large-scale quantum simulator on a diamond surface at room temperature, *Nat. Phys.* **9**, 168 (2013).
- [62] Z.-L. Xiang, S. Ashhab, J. Q. You, and F. Nori, Hybrid quantum circuits: Superconducting circuits interacting with other quantum systems, *Rev. Mod. Phys.* **85**, 623 (2013).
- [63] G. Kurizki, P. Bertet, Y. Kubo, K. Mølmer, D. Petrosyan, P. Rabl, and J. Schmiedmayer, Quantum technologies with hybrid systems, *Proc. Natl. Acad. Sci. U.S.A.* **112**, 3866 (2015).
- [64] M. Yu, P. Yang, M. Gong, Q. Cao, Q. Lu, H. Liu, S. Zhang, M. B. Plenio, F. Jelezko, T. Ozawa, N. Goldman, and J. Cai, Experimental measurement of the quantum geometric tensor using coupled qubits in diamond, *Nat. Sci. Rev.* **7**, 254 (2020).
- [65] M. Yu, Y. Liu, P. Yang, M. Gong, Q. Cao, S. Zhang, H. Liu, M. Heyl, T. Ozawa, N. Goldman, and J. Cai, Quantum Fisher information measurement and verification of the quantum Cramér–Rao bound in a solid-state qubit, *npj Quantum Inf.* **8**, 56 (2022).
- [66] M. Yu, D. Li, J. Wang, Y. Chu, P. Yang, M. Gong, N. Goldman, and J. Cai, Experimental estimation of the quantum Fisher information from randomized measurements, *Phys. Rev. Research* **3**, 043122 (2021).
- [67] P. Neumann, N. Mizuochi, F. Rempp, P. Hemmer, H. Watanabe, S. Yamasaki, V. Jacques, T. Gaebel, F. Jelezko, and J. Wrachtrup, Multipartite entanglement among single spins in diamond, *Science* **320**, 1326 (2008).
- [68] C. Zu, W.-B. Wang, L. He, W.-G. Zhang, C.-Y. Dai, F. Wang, and L.-M. Duan, Experimental realization of universal geometric quantum gates with solid-state spins, *Nature (London)* **514**, 72 (2014).
- [69] F. Jelezko and J. Wrachtrup, Single defect centres in diamond: A review, *Physica Status Solidi A* **203**, 3207 (2006).
- [70] M. W. Doherty, N. B. Manson, P. Delaney, F. Jelezko, J. Wrachtrup, and L. C. L. Hollenberg, The nitrogen-vacancy colour centre in diamond, *Phys. Rep.* **528**, 1 (2013).
- [71] G. Kucsko, P. C. Maurer, N. Y. Yao, M. Kubo, H. J. Noh, P. K. Lo, H. Park, and M. D. Lukin, Nanometre-scale thermometry in a living cell, *Nature (London)* **500**, 54 (2013).
- [72] V. M. Acosta, E. Bauch, M. P. Ledbetter, A. Waxman, L.-S. Bouchard, and D. Budker, Temperature dependence of the nitrogen-vacancy magnetic resonance in diamond, *Phys. Rev. Lett.* **104**, 070801 (2010).
- [73] P. Neumann, I. Jakobi, F. Dolde, C. Burk, R. Reuter, G. Waldherr, J. Honert, T. Wolf, A. Brunner, J. H. Shim, D. Suter, H. Sumiya, J. Isoya, and J. Wrachtrup, High-precision nanoscale temperature sensing using single defects in diamond, *Nano Lett.* **13**, 2738 (2013).
- [74] T. Plakhotnik, M. W. Doherty, J. H. Cole, R. Chapman, and N. B. Manson, All-optical thermometry and thermal properties of the optically detected spin resonances of the NV-center in nanodiamond, *Nano Lett.* **14**, 4989 (2014).
- [75] S. Knauer, J. P. Hadden, and J. G. Rarity, In-situ measurements of fabrication induced strain in diamond photonic-structures using intrinsic colour centres, *npj Quantum Inf.* **6**, 1 (2020).
- [76] M. E. Trusheim and D. Englund, Wide-field strain imaging with preferentially aligned nitrogen-vacancy centers in polycrystalline diamond, *New J. Phys.* **18**, 123023 (2016).
- [77] P. Kehayias, M. J. Turner, R. Trubko, J. M. Schloss, C. A. Hart, M. Wesson, D. R. Glenn, and R. L. Walsworth, Imaging crystal stress in diamond using ensembles of nitrogen-vacancy centers, *Phys. Rev. B* **100**, 174103 (2019).
- [78] F. Dolde, H. Fedder, M. W. Doherty, T. Nöbauer, F. Rempp, G. Balasubramanian, T. Wolf, F. Reinhard, L. C. L. Hollenberg, F. Jelezko, and J. Wrachtrup, Electric-field sensing using single diamond spins, *Nat. Phys.* **7**, 459 (2011).
- [79] J. R. Maze, P. L. Stanwix, J. S. Hodges, S. Hong, J. M. Taylor, P. Cappellaro, L. Jiang, M. V. Dutt, E. Togan, A. S. Zibrov, A. Yacoby, R. L. Walsworth, and M. D. Lukin, Nanoscale magnetic sensing with an individual electronic spin in diamond, *Nature (London)* **455**, 644 (2008).
- [80] G. Balasubramanian, I. Chan, R. Kolesov, M. Al-Hmoud, J. Tisler, C. Shin, C. Kim, A. Wojcik, P. R. Hemmer, A. Krueger, T. Hanke, A. Leitenstorfer, R. Bratschitsch, F. Jelezko, and J. Wrachtrup, Nanoscale imaging magnetometry with diamond spins under ambient conditions, *Nature (London)* **455**, 648 (2008).
- [81] P. Welter, J. Rhensius, A. Morales, M. S. Wörnle, C.-H. Lambert, G. Puebla-Hellmann, P. Gambardella, and C. L. Degen, Scanning nitrogen-vacancy center magnetometry in large in-plane magnetic fields, *Appl. Phys. Lett.* **120**, 074003 (2022).
- [82] J. Cai, F. Jelezko, and M. B. Plenio, Hybrid sensors based on colour centres in diamond and piezoelectric layers, *Nat. Commun.* **5**, 4065 (2014).
- [83] N. Wang, G.-Q. Liu, W.-H. Leong, H. Zeng, X. Feng, S.-H. Li, F. Dolde, H. Fedder, J. Wrachtrup, X.-D. Cui, S. Yang, Q. Li, and R.-B. Liu, Magnetic Criticality Enhanced Hybrid Nanodiamond Thermometer under Ambient Conditions, *Phys. Rev. X* **8**, 011042 (2018).
- [84] C.-F. Liu, W.-H. Leong, K. Xia, X. Feng, A. Finkler, A. Denisenko, J. Wrachtrup, Q. Li, and R.-B. Liu, Ultra-sensitive hybrid diamond nanothermometer, *Nat. Sci. Rev.* **8**, nwaa194 (2020).
- [85] Y. Liu and Z.-Y. Wang, Shortcuts to Adiabaticity with Inherent Robustness and without Auxiliary Control, *arXiv:2211.02543* (2022).
- [86] A. Carollo, M. F. Santos, and V. Vedral, Coherent Quantum Evolution via Reservoir Driven Holonomies, *Phys. Rev. Lett.* **96**, 020403 (2006).
- [87] A. Rivas and S. F. Huelga, *Open Quantum Systems* (Springer, Berlin, 2012).
- [88] See Supplemental Material for more details.
- [89] V. V. Dobrovitski, A. E. Feiguin, R. Hanson, and D. D. Awschalom, Decay of Rabi Oscillations by Dipolar-Coupled Dynamical Spin Environments, *Phys. Rev. Lett.* **102**, 237601 (2009).